Original Research Article

Investigating Nav1.6 and Its Potential Therapeutic Applications

Aiden Ashcraft

Edgemont Jr/Sr Highschool, 200 White Oak Ln, Scarsdale, NY 10583, United States

ABSTRACT

Neuropathic pain affects 6.9-10% of the global population, with first-line treatments providing meaningful relief in only ~30% of patients. Trafficking disruption has emerged as a therapeutic strategy for Nav1.7, where peptides disrupting the CRMP2-Nav1.7 interaction reduce channel surface expression and alleviate pain in preclinical models. This approach remains unexplored for Nav1.6 (SCN8A), despite regulatory protein interactions. This study evaluated whether Nav1.6 possesses molecular properties suitable for trafficking-based therapeutic modulation. We integrated transmembrane domain prediction (TMHMM), multiple sequence alignment across five species, protein-protein interaction network analysis (STRING), expression profiling (GTEx), and Hodgkin-Huxley modeling of dorsal root ganglion (DRG) neurons under varying Nav1.6 expression levels (1.0x normal, 1.5x neuropathic, 0.7x reduced, 0.1x knockout). Analysis revealed that MAP1B binding to the Nav1.6 N-terminus prevents endocytosis and controls surface expression, a regulatory mechanism similar to the CRMP2-Nav1.7 system, which has been successfully targeted for Nav1.7-mediated pain. Conservation analysis showed moderate variability in the MAP1B binding region (residues 77-80), contrasting with highly conserved transmembrane domains. Computational modeling demonstrated that ~30% Nav1.6 reduction (0.7x expression) eliminates repetitive firing while preserving normal responsiveness. Experimental MAP1B-Nav1.6 disruption achieves ~40% surface expression reduction, a magnitude that falls within the therapeutic range identified by the modeling, validating trafficking disruption as a therapeutic strategy. GTEx profiling confirmed CNS-enriched expressions. This computational integration predicts trafficking disruption as a therapeutic strategy for Nav1.6, with specific predictions directly testable in neuropathic pain models.

Keywords: Nav1.6; neuropathic pain; SCN8A; voltage-gated sodium channels; therapeutic target; trafficking disruption; MAP1B; computational modeling

INTRODUCTION

Neuropathic pain, arising from injury or dysfunction of the nervous system itself, represents one of the most challenging conditions in modern medicine, affecting approximately 6.9-10% of the global population (1). Unlike nociceptive pain, which serves as a protective warning signal, neuropathic pain persists long after initial tissue damage, characterized by spontaneous pain, allodynia (pain from normally non-painful stimuli), and hyperalgesia (increased sensitivity to painful stimuli) that can severely compromise quality of life. The underlying pathophysiology involves aberrant electrical activity in damaged sensory neurons, particularly in dorsal root ganglion (DRG) neurons that transmit pain signals from the periphery to the spinal cord.

Corresponding author: Aiden Ashcraft, E-mail: Aiden.l.ashcraft@gmail.com.

Accepted December 4, 2025
https://doi.org/10.70251/HYJR2348.36877894

Central to neuropathic pain pathogenesis is the dysregulation of voltage-gated sodium channels, which govern neuronal excitability and action potential generation. Among the nine mammalian sodium channel subtypes, Nav1.6 (encoded by SCN8A) has emerged as a particularly compelling therapeutic target due to its unique expression pattern and functional properties. Nav1.6 is concentrated at the axon initial segment and nodes of Ranvier in central neurons, where it supports rapid action-potential initiation and high-frequency firing (2). Critically, Nav1.6 contributes up to 60% of tetrodotoxin-sensitive sodium current in large DRG neurons, the primary mediators of mechanical and thermal sensation (3).

Recent experimental evidence has established Nav1.6's crucial role in neuropathic pain states. Chen *et al* (3) demonstrated that Nav1.6 knockout ameliorates neuropathic pain in animal models, while accumulation of Nav1.6 channels at sites of nerve injury contributes to the hyperexcitability characteristic of damaged sensory neurons. Furthermore, the channel's involvement extends beyond mechanical injury to chemotherapy-induced peripheral neuropathy, a painful side effect affecting cancer patients (4). The recognition of Nav1.6's role has prompted pharmaceutical development, with the Nav1.6-selective inhibitor NBI-921352 currently in Phase II clinical trials for epilepsy (5).

Despite growing recognition of Nav1.6's role in neuropathic pain, alternative therapeutic modalities beyond direct channel blockade have not been systematically explored. In contrast, Nav1.7 research has investigated trafficking disruption as a therapeutic strategy: peptides disrupting the CRMP2-Nav1.7 interaction reduce channel surface expression through endocytosis modulation and alleviate pain in preclinical models (8-10). The relatively small amount of Nav1.6 research reflects not limitations but rather the recent recognition of its pain-relevant functions. Current neuropathic pain treatments remain inadequate, with first-line therapies including gabapentinoids achieving meaningful pain relief (≥50% pain reduction) in approximately 30-35% of patients, leaving the majority with inadequate symptom control (6, 7). The persistent unmet medical need underscores the importance of investigating new targets like Nav1.6.

Nav1.6 has been shown to engage in regulatory interactions that control surface expression. Specifically, MAP1B (microtubule-associated protein 1B) binds to the Nav1.6 N-terminus (residues 77-80, VAVP motif) and prevents endocytosis at the axon initial segment, thereby maintaining channel surface availability (11, 12). Disruption of this interaction increases Nav1.6 endocytosis and substantially reduces surface expression at the axon initial segment (12). Despite this characterized regulatory mechanism and its functional similarity to the Nav1.7-CRMP2 system, trafficking disruption has not been proposed as a therapeutic approach for Nav1.6-mediated neuropathic pain.

This study systematically characterizes Nav1.6's structural, evolutionary, and functional properties through computational integration to establish that trafficking disruption represents a viable therapeutic strategy for Nav1.6, using the established Nav1.7-CRMP2 trafficking disruption approach as a guide.

METHODS AND MATERIALS

Study Design

This in-silico investigation employed multiple bioinformatics and modeling approaches to study Nav1.6 (SCN8A) as a therapeutic target for neuropathic pain. The study integrated transmembrane domain prediction (TMHMM), multiple sequence alignment, protein interaction network analysis (STRING), expression profiling (GTEx), and Hodgkin-Huxley neuronal modeling to assess the molecular feasibility of trafficking-based modulation. Specifically, the analysis encompassed: (A) structural and evolutionary analysis of Nav1.6 protein architecture, (B) protein-protein interaction network mapping, (C) expression profiling across human tissues, and (D) computational modeling of dorsal root ganglion (DRG) neuron excitability under varying Nav1.6 expression conditions.

Bioinformatics databases and software

This study utilized multiple bioinformatics databases and computational tools for structural analysis, sequence conservation studies, protein interaction mapping, and expression profiling. Protein sequences, gene annotations, and relevant literature for SCN8A were retrieved through the National Center for Biotechnology Information (NCBI), while UniProt provided detailed information on the human Nav1.6 protein (UniProt ID: Q9UQD0), including functional domains and post-translational modifications. Genomic coordinates, transcript variants, and regulatory features of SCN8A were obtained from Ensembl. Bulk tissue expression patterns were evaluated using GTEx data accessed through the MARRVEL platform, which also facilitated cross-species functional annotation. To characterize structural features,

transmembrane helices were predicted using the TMHMM Server v2.0, and evolutionary conservation was examined through multiple sequence alignment performed with Clustal Omega under default settings. Protein–protein interaction networks were explored using STRING v12.0 with a medium confidence threshold (0.4).

Transmembrane domain analysis

Nav1.6's protein sequence was analyzed using TMHMM Server v2.0 to predict transmembrane helices. The algorithm employs a hidden Markov model trained on experimentally verified transmembrane proteins to identify membrane-spanning regions, cytoplasmic domains, and extracellular loops. Posterior probabilities were calculated for each residue position across three states: transmembrane, inside (cytoplasmic), and outside (outside of membrane layer). Note that TMHMM predictions may not resolve all transmembrane segments in complex multi-domain proteins, and results should be interpreted within the context of established structural knowledge.

Evolutionary conservation analysis

Multiple sequence alignment was performed using Clustal Omega with Nav1.6 from representative species: Homo sapiens, Mus musculus, Rattus norvegicus, Danio rerio, and Drosophila melanogaster. Protein sequences were retrieved from NCBI and aligned using default parameters (gap opening penalty: 11, gap extension penalty: 1). Conservation scoring identified functionally critical domains and potential therapeutic targeting sites.

Protein-Protein Interaction network analysis

STRING database v12.0 was used to construct Nav1.6-centered interaction networks. Analysis parameters included: organism Homo sapiens, confidence threshold 0.4 (medium), maximum interactions 50. Evidence channels included experimental data, co-expression, text mining, and database annotations. Networks were visualized to identify functional clusters including scaffolding proteins (ankyrin-G, spectrin), auxiliary subunits, and regulatory factors.

Expression profiling

SCN8A expression data was extracted from GTEx v8 via the MARRVEL database, encompassing 54 human tissue types with 17,382 samples total. Transcript abundance was measured as Transcripts Per Million (TPM) with violin plots showing distribution statistics. Tissue specificity analysis identified CNS enrichment patterns relevant to therapeutic targeting strategies.

Computational neuron modeling

DRG neuron models were implemented in Python (version 3.8) using NumPy (version 1.21.0) for numerical computations, Matplotlib (version 3.4.3) for visualization, and SciPy (version 1.7.0) for numerical integration, and established Hodgkin-Huxley formulations (13, 14).

The Hodgkin-Huxley computational model employed several simplifying assumptions that should be considered when interpreting results. First, the model assumes uniform distribution of Nav1.6 channels across the neuronal membrane, whereas experimental evidence demonstrates that Nav1.6 channels cluster at specific subcellular locations including the axon initial segment and nodes of Ranvier (2). This spatial heterogeneity influences action potential initiation and propagation patterns in real neurons.

Second, the model focuses exclusively on Nav1.6 channels while DRG neurons express multiple sodium channel subtypes (Nav1.1, Nav1.6, Nav1.7, Nav1.8, and Nav1.9) that contribute differentially to neuronal excitability. The relative contributions of these channels vary with cell size, developmental stage, and pathological conditions, creating a more complex excitability profile than captured by the single-channel model.

Third, the simulation employs static parameters throughout the modeling period, whereas neuropathic pain involves dynamic changes in channel expression, localization, and biophysical properties over time. Real neuropathic conditions feature ongoing inflammatory processes, altered gene expression, and progressive changes in neuronal morphology that this steady-state model cannot capture.

Finally, the model uses simplified neuronal morphology without dendritic arbors or realistic axonal geometry, which influence current distribution and spike propagation. Despite these limitations, the model provides valuable insights into the relationship between Nav1.6 expression levels and basic excitability patterns, serving as a foundation for understanding more complex physiological interactions.

DRG neuron models were implemented in Python using standard Hodgkin–Huxley–type formulations. The membrane was represented with a capacitance of 1.0 μF/cm² and included a passive leak current with a conductance of 0.0001 mS/cm² and a reversal potential of –65 mV. Active conductances consisted of delayed rectifier potassium channels (0.036 mS/cm²; reversal

potential –90 mV) and voltage-gated sodium channels representing Nav1.6, whose maximal conductance was varied to reflect different expression states. Nav1.6 currents were modeled with a maximum conductance of 0.120 mS/cm² under normal expression and a reversal potential of +50 mV. Activation kinetics followed voltage-dependent rate constants derived from experimental literature, while inactivation was represented using fast inactivation time constants reported in previous physiological studies. To examine the effects of altered channel density, four Nav1.6 expression conditions were simulated: normal expression (1.0× baseline, 0.120 mS/cm²), neuropathic high expression (1.5×, 0.180 mS/cm²), neuropathic low expression (0.7×, 0.084 mS/cm²), and a near-knockout condition (0.1×, 0.012 mS/cm²). Each simulation was run for 100 ms, with a depolarizing stimulus delivered from 20 to 80 ms (60 ms total duration) at a current amplitude of 5.0 pA/cm². The integration time step was 0.01 ms to ensure numerical stability and temporal precision.

Quantitative electrophysiological measures were extracted from each simulation to characterize neuronal excitability under varying Nav1.6 expression levels. Action potentials were identified using a spike-detection threshold of –10 mV, allowing reliable discrimination of suprathreshold events. Firing frequency was calculated as the total number of detected spikes during the 60-ms stimulation window. Additional metrics included the peak membrane voltage, defined as the maximum membrane potential achieved during stimulation, and the overall voltage range, computed as the difference between the maximum and minimum membrane potentials within each trial. To assess sodium channel contribution directly, the average inward Nav1.6 current across the stimulus period was also quantified.

RESULTS

Nav1.6 transmembrane domain prediction reveals expected sodium channel architecture

To better understand how Nav1.6 contributes to dorsal root ganglion cell excitability, it is essential to examine its structural organization and subcellular localization. Nav1.6 is a large voltage-gated sodium channel encoded by SCN8A, spanning nearly 2000 amino acids, and its transmembrane organization is critical for proper channel function and localization. TMHMM (Transmembrane Hidden Markov Model) analysis was performed, a widely used hidden Markov model-based method for predicting transmembrane helices. This analysis maps which regions of the protein are embedded in the lipid bilayer, which are cytoplasmic, and which are outside the membrane layer. Such predictions provide structural context for interpreting channel gating and potential molecular interventions.

The TMHMM analysis predicted multiple transmembrane segments organized in the expected clustered pattern consistent with voltage-gated sodium channel architecture (Figure 1 and Figure 2). However, the algorithm predicted 19 transmembrane segments, which differs from the established 24-segment architecture (4 domains × 6 segments each) confirmed by structural studies of Nav1.6 and related sodium channels. This discrepancy likely reflects limitations in TMHMM's ability to resolve closely spaced transmembrane regions in multi-domain membrane proteins rather than the actual protein structure. The overall topological pattern showing four distinct clusters of transmembrane predictions with appropriate inside/outside alternations confirms that Nav1.6 conforms to the canonical sodium channel architecture, consistent with its structural suitability as a molecular target in DRGs.

Multiple protein alignment of Nav1.6 across multiple species reveals conserved amino acids

To investigate evolutionary conservation and functional importance of voltage-gated sodium channel Nav1.6 (encoded by SCN8A), a multiple sequence alignment was performed of its protein sequence across different species (Figure 3). Nav1.6 plays a crucial role in the initiation and propagation of action potentials in DRGs and other neurons, particularly at the axon initial segment and nodes of Ranvier (2). Understanding which amino acids are conserved across species can reveal residues critical for the structural stability and gating mechanism of the channel. Highly conserved regions often correspond to essential functional domains, such as the voltage-sensing segments and pore-forming loops, which are critical for sodium selectivity and fast activation/inactivation. Highly conserved regions (>95% identity) should be avoided as therapeutic targets due to high probability of disrupting essential channel function, whereas moderately conserved regulatory domains like the MAP1B binding site may tolerate selective disruption for trafficking-based modulation. High sequence conservation across species supports the validity of animal models in translational research.

The presence of large blocks of conserved amino acids in the transmembrane domains and pore regions highlights their essential role in Nav1.6 function, as

```
# sp|Q9UQD0.1|SCN8A_HUMAN Length: 1980
# sp|Q9UQD0.1|SCN8A_HUMAN Number of predicted TMHs:  19
# sp|Q9UQD0.1|SCN8A_HUMAN Exp number of AAs in TMHs: 489.0012
# sp|Q9UQD0.1|SCN8A_HUMAN Exp number, first 60 AAs:  5e-05
# sp|Q9UQD0.1|SCN8A_HUMAN Total prob of N-in:        0.35666
sp|Q9UQD0.1|SCN8A_HUMAN TMHMM2.0        inside       1   128
sp|Q9UQD0.1|SCN8A_HUMAN TMHMM2.0        TMhelix    129   151
sp|Q9UQD0.1|SCN8A_HUMAN TMHMM2.0        outside    152   193
sp|Q9UQD0.1|SCN8A_HUMAN TMHMM2.0        TMhelix    194   216
sp|Q9UQD0.1|SCN8A_HUMAN TMHMM2.0        inside     217   222
sp|Q9UQD0.1|SCN8A_HUMAN TMHMM2.0        TMhelix    223   245
sp|Q9UQD0.1|SCN8A_HUMAN TMHMM2.0        outside    246   254
sp|Q9UQD0.1|SCN8A_HUMAN TMHMM2.0        TMhelix    255   277
sp|Q9UQD0.1|SCN8A_HUMAN TMHMM2.0        inside     278   388
sp|Q9UQD0.1|SCN8A_HUMAN TMHMM2.0        TMhelix    389   411
sp|Q9UQD0.1|SCN8A_HUMAN TMHMM2.0        outside    412   748
sp|Q9UQD0.1|SCN8A_HUMAN TMHMM2.0        TMhelix    749   771
sp|Q9UQD0.1|SCN8A_HUMAN TMHMM2.0        inside     772   783
sp|Q9UQD0.1|SCN8A_HUMAN TMHMM2.0        TMhelix    784   806
sp|Q9UQD0.1|SCN8A_HUMAN TMHMM2.0        outside    807   870
sp|Q9UQD0.1|SCN8A_HUMAN TMHMM2.0        TMhelix    871   893
sp|Q9UQD0.1|SCN8A_HUMAN TMHMM2.0        inside     894   953
sp|Q9UQD0.1|SCN8A_HUMAN TMHMM2.0        TMhelix    954   976
sp|Q9UQD0.1|SCN8A_HUMAN TMHMM2.0        outside    977  1197
sp|Q9UQD0.1|SCN8A_HUMAN TMHMM2.0        TMhelix   1198  1217
sp|Q9UQD0.1|SCN8A_HUMAN TMHMM2.0        inside    1218  1237
sp|Q9UQD0.1|SCN8A_HUMAN TMHMM2.0        TMhelix   1238  1260
sp|Q9UQD0.1|SCN8A_HUMAN TMHMM2.0        outside   1261  1269
sp|Q9UQD0.1|SCN8A_HUMAN TMHMM2.0        TMhelix   1270  1292
sp|Q9UQD0.1|SCN8A_HUMAN TMHMM2.0        inside    1293  1318
sp|Q9UQD0.1|SCN8A_HUMAN TMHMM2.0        TMhelix   1319  1341
sp|Q9UQD0.1|SCN8A_HUMAN TMHMM2.0        outside   1342  1441
sp|Q9UQD0.1|SCN8A_HUMAN TMHMM2.0        TMhelix   1442  1464
sp|Q9UQD0.1|SCN8A_HUMAN TMHMM2.0        inside    1465  1525
sp|Q9UQD0.1|SCN8A_HUMAN TMHMM2.0        TMhelix   1526  1543
sp|Q9UQD0.1|SCN8A_HUMAN TMHMM2.0        outside   1544  1552
sp|Q9UQD0.1|SCN8A_HUMAN TMHMM2.0        TMhelix   1553  1571
sp|Q9UQD0.1|SCN8A_HUMAN TMHMM2.0        inside    1572  1583
sp|Q9UQD0.1|SCN8A_HUMAN TMHMM2.0        TMhelix   1584  1606
sp|Q9UQD0.1|SCN8A_HUMAN TMHMM2.0        outside   1607  1653
sp|Q9UQD0.1|SCN8A_HUMAN TMHMM2.0        TMhelix   1654  1676
sp|Q9UQD0.1|SCN8A_HUMAN TMHMM2.0        inside    1677  1742
sp|Q9UQD0.1|SCN8A_HUMAN TMHMM2.0        TMhelix   1743  1765
sp|Q9UQD0.1|SCN8A_HUMAN TMHMM2.0        outside   1766  1980
```

Figure 1. TMHMM analysis output for Nav1.6 transmembrane prediction. Raw TMHMM (Transmembrane Hidden Markov Model) prediction output for human Nav1.6 protein (UniProt ID: Q9UQD0). The output displays: protein identifier (sp|Q9UQD0.1|SCN8A_HUMAN), total sequence length (1980 amino acids), number of predicted transmembrane helices (TMHs: 19), expected number of amino acids in TMHs (489.0012), and expected number of amino acids in the first 60 residues (5e-05). The subsequent lines show position-by-position predictions across the entire protein sequence, with each residue classified as either "inside" (cytoplasmic), "TMhelix" (transmembrane helix), or "outside" (extracellular/lumenal). The numerical ranges indicate the amino acid positions for each predicted structural state. While TMHMM predicted 19 transmembrane segments due to algorithmic limitations in resolving closely spaced helices, this data provides the foundation for understanding Nav1.6's membrane topology and is visualized graphically in Figure 2.

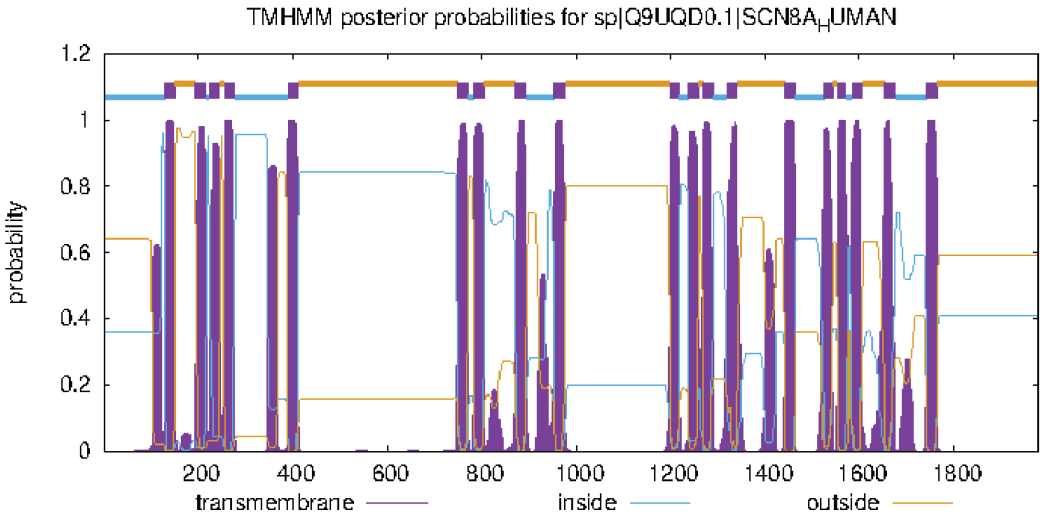

Figure 2. Graphical representation of Nav1.6 transmembrane domain. Posterior probability plot showing TMHMM predictions for Nav1.6 structural states across the full protein sequence. The x-axis represents the amino acid sequence from N-terminus (left) to C-terminus (right), spanning residues 1-1980. The y-axis indicates the posterior probability (0-1.0) that a given residue belongs to a particular structural state. The three-color traces correspond to predicted regions: purple denotes transmembrane helices (α-helical segments embedded within the lipid bilayer), blue indicates residues predicted to be located on the cytoplasmic side (inside), and yellow indicates residues predicted to be outside of the membrane layer (extracellular or luminal). Peaks in the purple trace mark transmembrane helices, and the model identifies multiple transmembrane helices organized in four distinct clusters corresponding to the four homologous domains (I-IV) characteristic of voltage-gated sodium channels. The alternating inside-outside predictions between transmembrane segments validate the expected membrane topology. This pattern corresponds to the canonical four-domain sodium channel structure, each containing six membrane-spanning segments for a total of 24 transmembrane segments, though TMHMM's resolution limitations result in 19 predicted segments as detailed in Figure 1.

```
CLUSTAL O(1.2.4) multiple sequence alignment


zebrafish_XP_068072896.1        MAAPLLAPPGPNSYKYFTRESLREIEKRIEEEKAKPPPKPDNSYRDDDDENKPKPNGDLE 60
frog_XP_031751845.1             MAAPLMAPPGPDSFKAFTRESLAAIEKRIAEEKNKKPPKQDSSHRDDDDENKPRPNSDLE 60
human_sp|Q9UQD0.1|SCN8A_HUMAN   MAARLLAPPGPDSFKPFTPESLANIERRIAESKLKKPPKADGSHREDDEDSKPKPNSDLE 60
mouse_sp|Q9WTU3.1|SCN8A_MOUSE   MAARVLAPPGPDSFKPFTPESLANIERRIAESKLKKPPKADGSHREDDEDSKPKPNSDLE 60
                                *** ::*****:*:* ** ***  **:** *.* * *** *.*:*:**::.**:**.***

zebrafish_XP_068072896.1        AGKSLPFIYGDIPPGMVATPLEDFDPFYINQKTFVVLNKGKTIFRFSATPALYMISPFNL 120
frog_XP_031751845.1             AGKGVPFIYGDCPSRLIAEPIEDLDPFYLHTKTFIVLNRGKTIFRFSAAPALYILSPFNP 120
human_sp|Q9UQD0.1|SCN8A_HUMAN   AGKSLPFIYGDIPQGLVAVPLEDFDPYYLTQKTFVVLNRGKTLFRFSATPALYILSPFNL 120
mouse_sp|Q9WTU3.1|SCN8A_MOUSE   AGKSLPFIYGDIPQGLVAVPLEDFDPYYLTQKTFVVLNRGKTLFRFSATPALYILSPFNL 120
                                ***.:****** *  ::* *:**:**:*:  ***:***:***:*****:****::****

zebrafish_XP_068072896.1        ARRIAIKILIHSVFSMFIMCTILTNCVFMTFSNPPEWSKQVEYTFTGIYTFESAVKIIAR 180
frog_XP_031751845.1             LRKFAIKILIHSLFSMIIMCTILTNCVFMTFSNPPEWSKQVEYTFTGIYTFESLVKIIAR 180
human_sp|Q9UQD0.1|SCN8A_HUMAN   IRRIAIKILIHSVFSMIIMCTILTNCVFMTFSNPPDWSKNVEYTFTGIYTFESLVKIIAR 180
mouse_sp|Q9WTU3.1|SCN8A_MOUSE   IRRIAIKILIHSVFSMIIMCTILTNCVFMTFSNPPEWSKNVEYTFTGIYTFESLVKIIAR 180
                                 *::********:***:******************:***:************* ******
```

```
zebrafish_XP_068072896.1        ATMEEAERKEAEFKAMLEQLKKQQEDAQANAMATSAGTVSEDVVEDDGDGEGNLSCSSSE 480
frog_XP_031751845.1             ATLEEAERKENEFKAMLEQMKRMQEEAQAAANATSAGTVTEDAVEDEDGEAR-MSHTSSE 478
human_sp|Q9UQD0.1|SCN8A_HUMAN   ATLEEAEQKEAEFKAMLEQLKKQQEEAQAAAMATSAGTVSEDAIEEEGEEGGGSPRSSSE 479
mouse_sp|Q9WTU3.1|SCN8A_MOUSE   ATLEEAEQKEAEFKAMLEQLKKQQEEAQAAAMATSAGTVSEDAIEEEGEDGVGSPRSSSE 479
                                **:****:** ********:*: **:*** * *******:**.:*::.        :***

zebrafish_XP_068072896.1        MSKLSSKSAKERRNRKKKWRQKE--QDKEKGDSEKFVKSESDDGSR-RRFRFPDNRLGRR 537
frog_XP_031751845.1             FSKPSSKSAKERRNRRKKRKQKELSEGEEKGDSEKVYKSESEDGVKRRGFWYPDNRLGRR 538
human_sp|Q9UQD0.1|SCN8A_HUMAN   ISKLSSKSAKERRNRRKKRKQKELSEGEEKGDPEKVFKSESEDGMRRKAFRLPDNRIGRK 539
mouse_sp|Q9WTU3.1|SCN8A_MOUSE   LSKLSSKSAKERRNRRKKRKQKELSEGEEKGDPEKVFKSESEDGMRRKAFRLPDNRIGRK 539
                                :** ***********:** :***  :.:**** **. ****:** : : *  ****:**:

zebrafish_XP_068072896.1        SSIMNQSLLSIPGSPFPSRRNSKSSIFS-----RCKDGGSENEFADDEHSTVEEYDERRD 592
frog_XP_031751845.1             FSIMNQSLLSIPGSPYLSRHNSKSSIFSFR--GRFRDPVSENEFADDEHSTVEESEGRRD 596
human_sp|Q9UQD0.1|SCN8A_HUMAN   FSIMNQSLLSIPGSPFLSRHNSKSSIFSFRGPGRFRDPGSENEFADDEHSTVEESEGRRD 599
mouse_sp|Q9WTU3.1|SCN8A_MOUSE   FSIMNQSLLSIPGSPFLSRHNSKSSIFSFRGPGRFRDPGSENEFADDEHSTVEESEGRRD 599
                                 **************: **:********     * :*  *************** : ***

zebrafish_XP_068072896.1        SFLSPQ----RRSSYTGFYG-----------------KRNSTVDCNGVVSLIGP----G 626
frog_XP_031751845.1             SLFIPVRGHDRRNSYN--SGYSQGSRSSRILQNLRRNPKRNSTVDCNGVVSLIGGPGSNI 654
human_sp|Q9UQD0.1|SCN8A_HUMAN   SLFIPIRARERRSSYSGYSGYSQGSRSSRIFPSLRRSVKRNSTVDCNGVVSLIGGPGSHI 659
mouse_sp|Q9WTU3.1|SCN8A_MOUSE   SLFIPIRARERRSSYSGYSGYSQCSRSSRIFPSLRRSVKRNSTVDCNGVVSLIG-PGSHI 658
                                *:: *     **.**.   *                 ***************

zebrafish_XP_068072896.1        PGGRLLPEVIIDKAATDDSPTTDLEIKKKLSGSLMVSVEQLNTSFGRKERANSVMSALTN 686
frog_XP_031751845.1             PGGRLLPEVKIDKAATDDSPTTEVEVKRKPSGSLRVSMDQLTAS-FGRKRANSILSVVTQ 713
human_sp|Q9UQD0.1|SCN8A_HUMAN   G-GRLLPEA-----------TTEVEIKKKGPGSLLVSMDQLASY-GRKDRINSIMSVVTN 706
mouse_sp|Q9WTU3.1|SCN8A_MOUSE   --GRLLPEA-----------TTEVEIKKKGPGSLLVSMEQLASY-GRKDRINSIMSVVTN 704
                                  ******.           **::*:*:*  *** **::** :    :.* **::*.:*:

zebrafish_XP_068072896.1        TLVEELEESQRKCPPCWYKFANTFLIWECGPLWMSIKEIVNLIVMDPFVDLAITICIVLN 746
frog_XP_031751845.1             TLVEELEESQRKCPPCWYKFADTYLIWTCCPLWIRIKTIVNMIVMDPFVDLTITICIVLN 773
human_sp|Q9UQD0.1|SCN8A_HUMAN   TLVEELEESQRKCPPCWYKFANTFLIWECHPYWIKLKEIVNLIVMDPFVDLAITICIVLN 766
mouse_sp|Q9WTU3.1|SCN8A_MOUSE   TLVEELEESQRKCPPCWYKFANTFLIWECHPYWIKLKEIVNLIVMDPFVDLAITICIVLN 764
                                **********************:*:*** * * *: :* ***:*********:********

zebrafish_XP_068072896.1        TLFMAMEHYPMTPQFEHVLSVGNLVFTGIFTAEMFAKLVAMDPYYYFQEGWNIFDGFIVS 806
frog_XP_031751845.1             TLFMAMEHYPMTPHFENVLVVGNLVFTGIFTAEMFLKLIAMDPYYYFQEGWNIFDGFIVS 833
human_sp|Q9UQD0.1|SCN8A_HUMAN   TLFMAMEHHPMTPQFEHVLAVGNLVFTGIFTAEMFLKLIAMDPYYYFQEGWNIFDGFIVS 826
mouse_sp|Q9WTU3.1|SCN8A_MOUSE   TLFMAMEHHPMTPQFEHVLAVGNLVFTGIFTAEMFLKLIAMDPYYYFQEGWNIFDGFIVS 824
                                ********:****:**:** *************** **:**********************

zebrafish_XP_068072896.1        LSLMELGLANVEGLSVLRSFRLLRVFKLAKSWPTLNMLIKIIGNSVGALGNLTLVLAIIV 866
frog_XP_031751845.1             LSLMELGLQDVEGLSVLRSFRLLRVFKLAKSWPTLNMLIKIIGNSVGALGNLTLVLAIIV 893
human_sp|Q9UQD0.1|SCN8A_HUMAN   LSLMELSLADVEGLSVLRSFRLLRVFKLAKSWPTLNMLIKIIGNSVGALGNLTLVLAIIV 886
mouse_sp|Q9WTU3.1|SCN8A_MOUSE   LSLMELGLADVEGLSVLRSFRLLRVFKLAKSWPTLNMLIKIIGNSVGALGNLTLVLAIIV 884
                                ******.* :************************************************
```

```
zebrafish_XP_068072896.1        FIFAVVGMQLFGKSYKDCVCKIAQDCELPRWHMNDFFHSFLIVFRVLCGEWIETMWDCME 926
frog_XP_031751845.1             FIFAVVGMQLFGKSYKDCVCKINPECVLPRWHMNDFFHSFLIVFRVLCGEWIETMWDCME 953
human_sp|Q9UQD0.1|SCN8A_HUMAN   FIFAVVGMQLFGKSYKECVCKINQDCELPRWHMHDFFHSFLIVFRVLCGEWIETMWDCME 946
mouse_sp|Q9WTU3.1|SCN8A_MOUSE   FIFAVVGMQLFGKSYKECVCKISQECKLPRWHMNDFFHSFLIVFRVLCGEWIETMWDCME 944
                                ***************:*****  :* ******:************************

zebrafish_XP_068072896.1        VAGQAMCLIVFMMVMVIGNLVVLNLFLALLLSSFSADNLAASDDDGEMNNLQIAVIRIKK 986
frog_XP_031751845.1             VAGQAMCIIVFMMVMVIGNLVVLNLFLALLLSSFSADNLAATDDDGEMNNLQISVIRIKK 1013
human_sp|Q9UQD0.1|SCN8A_HUMAN   VAGQAMCLIVFMMVMVIGNLVVLNLFLALLLSSFSADNLAATDDDGEMNNLQISVIRIKK 1006
mouse_sp|Q9WTU3.1|SCN8A_MOUSE   VAGQAMCLIVFMMVMVIGNLVVLNLFLALLLSSFSADNLAATDDDGEMNNLQISVIRIKK 1004
                                *******:**********************************:***********:******

zebrafish_XP_068072896.1        GIAWVKAKVRELVNIILGRKVTDEAKPLDDMYDRKLNCIANHTGVDISRDLDYQKNGNGT 1046
frog_XP_031751845.1             GIAWIKLKAHDFMQKHFKKKDADEVKPLDEMYEKKMNCLANNTGADIHRDMDYPKNGNGT 1073
human_sp|Q9UQD0.1|SCN8A_HUMAN   GVAWTKLKVHAFMQAHFKQREADEVKPLDELYEKKANCIANHTGADIHRNGDFQKNGNGT 1066
mouse_sp|Q9WTU3.1|SCN8A_MOUSE   GVAWAKVKVHAFMQAHFKQREADEVKPLDELYEKKANCIANHTGVDIHRNGDFQKNGNGT 1064
                                *:** * *.: :::  : :: :**.****::*::* **:**:**.** *: *: ******

zebrafish_XP_068072896.1        TSGIGSSVGKYMIDDDHMSFIHNPNLTVCVPIAVGESDFENLNTEDFSSESEAEGSK-EL 1105
frog_XP_031751845.1             TSGIGSSVEKYMIDEDHMSFIHNPNLTVKVPIAVGESDFENLNTEDFSSASDEEGSKDKL 1133
human_sp|Q9UQD0.1|SCN8A_HUMAN   TSGIGSSVEKYIIDEDHMSFINNPNLTVRVPIAVGESDFENLNTEDVSSESDPEGSKDKL 1126
mouse_sp|Q9WTU3.1|SCN8A_MOUSE   TSGIGSSVEKYIIDEDHMSFINNPNLTVRVPIAVGESDFENLNTEDVSSESDPEGSKDKL 1124
                                ******** **:**:******:****** ****************.** *: **** :*

zebrafish_XP_068072896.1        DDISSSEGSTIDIKPEVEEAVVVETVEEYVDPEACWTEACIARYKCCDVPITEGWGKNWW 1165
frog_XP_031751845.1             DDTSSSEGSTIDIKPEAEEV-PVEQPEEYLDPDNCFTEGCVARFKCCQVSVEEGLGKSWW 1192
human_sp|Q9UQD0.1|SCN8A_HUMAN   DDTSSSEGSTIDIKPEVEEV-PVEQPEEYLDPDACFTEGCVQRFKCCQVNIEEGLGKSWW 1185
mouse_sp|Q9WTU3.1|SCN8A_MOUSE   DDTSSSEGSTIDIKPEVEEV-PVEQPEEYLDPDACFTEGCVQRFKCCQVNIEEGLGKSWW 1183
                                ** ************.**.  **  ***:**: *:**.*: *:***:* : ** **.**

zebrafish_XP_068072896.1        FLRKTCYLIVEHNWFETLIIFMILLSSGALAFEDVYIEQRKTIRIILEYADMVFTYIFIL 1225
frog_XP_031751845.1             TLRKTCFLIVEHNWFETFIIFMILLSSGALAFEDVYIEQRKTIRTILEYADKVFTYIFIL 1252
human_sp|Q9UQD0.1|SCN8A_HUMAN   ILRKTCFLIVEHNWFETFIIFMILLSSGALAFEDIYIEQRKTIRTILEYADKVFTYIFIL 1245
mouse_sp|Q9WTU3.1|SCN8A_MOUSE   ILRKTCFLIVEHNWFETFIIFMILLSSGALAFEDIYIEQRKTIRTILEYADKVFTYIFIL 1243
                                 *****:**********:***************:********* ****** ********

zebrafish_XP_068072896.1        EMLLKWVAYGFVKYFTNAWCWLDFFIVDVSIVSLIANALGYSDLGPIKSLRTLRALRPLR 1285
frog_XP_031751845.1             EMLLKWLAYGFVKFFTNAWCWLDFLIVDVSLVSLIANALGYSELGAIKSLRTLRALRPLR 1312
human_sp|Q9UQD0.1|SCN8A_HUMAN   EMLLKWTAYGFVKFFTNAWCWLDFLIVAVSLVSLIANALGYSELGAIKSLRTLRALRPLR 1305
mouse_sp|Q9WTU3.1|SCN8A_MOUSE   EMLLKWTAYGFVKFFTNAWCWLDFLIVAVSLVSLIANALGYSELGAIKSLRTLRALRPLR 1303
                                ****** ******:**********:** **:***********:** **************

zebrafish_XP_068072896.1        ALSRFEGMRVVVNALVGAIPSIMNVLLVCLIFWLIFSIMGVNMFAGKYYYCYNETEKAYF 1345
frog_XP_031751845.1             ALSRFEGMRVVVNALVGAIPSIMNVLLVCLIFWLIFSIMGVNLFAGKYYYCYNETAEGMF 1372
human_sp|Q9UQD0.1|SCN8A_HUMAN   ALSRFEGMRVVVNALVGAIPSIMNVLLVCLIFWLIFSIMGVNLFAGKYHYCFNETSEIRF 1365
mouse_sp|Q9WTU3.1|SCN8A_MOUSE   ALSRFEGMRVVVNALVGAIPSIMNVLLVCLIFWLIFSIMGVNLFAGKYHYCFNETSEIRF 1363
                                ******************************************:*****:**:*** :  *
```

```
zebrafish_XP_068072896.1        ELDVVNNKSECFALIEQNYTEVRWKNVKINFDNVGAGYLALLQVATFKGWMDIMYAAVDS 1405
frog_XP_031751845.1             EIEDVENETQCFDLIGNNYTEVRWKNVKINFDNVGAGYLALLQVATFKGWMDIMYAAVDS 1432
human_sp|Q9UQD0.1|SCN8A_HUMAN   EIEDVNNKTECEKLMEGNNTEIRWKNVKINFDNVGAGYLALLQVATFKGWMDIMYAAVDS 1425
mouse_sp|Q9WTU3.1|SCN8A_MOUSE   EIDEVNNKTDCEKLMEGNNTEIRWKNVKINFDNVGAGYLALLQVATFKGWMDIMYAAVDS 1423
                                *:: *:*:::*  *:  * **:************************************

zebrafish_XP_068072896.1        RRVEDQPKYEDNIYMYIYFVIFIIFGSFFTLNLFIGVIIDNFNQQKKKFGGQDIFMTEEQ 1465
frog_XP_031751845.1             RKVHQQPKYEDNIYMYIYFVIFIIFGSFFTLNLFIGVIIDNFNQQKKKFGGQDIFMTEEQ 1492
human_sp|Q9UQD0.1|SCN8A_HUMAN   RKPDEQPKYEDNIYMYIYFVIFIIFGSFFTLNLFIGVIIDNFNQQKKKFGGQDIFMTEEQ 1485
mouse_sp|Q9WTU3.1|SCN8A_MOUSE   RKPDEQPDYEGNIYMYIYFVIFIIFGSFFTLNLFIGVIIDNFNQQKKKFGGQDIFMTEEQ 1483
                                *: .:**.**.************************************************

zebrafish_XP_068072896.1        KKYYNAMKKLGSKKPQKPIPRPQNKLQGMVFDFVTQQVFDISIMILICLNMVTMMVETDD 1525
frog_XP_031751845.1             KKYYNAMKKLGSKKPQKPIPRPLNKFQGAIFDIITQQAFDIVIMILICLNMVTMMVETDD 1552
human_sp|Q9UQD0.1|SCN8A_HUMAN   KKYYNAMKKLGSKKPQKPIPRPLNKIQGIVFDFVTQQAFDIVIMMLICLNMVTMMVETDT 1545
mouse_sp|Q9WTU3.1|SCN8A_MOUSE   KKYYNAMKKLGSKKPQKPIPRPLNKIQGIVFDFVTQQAFDIVIMMLICLNMVTMMVETDT 1543
                                ********************** **:** :**::***.*** **:**************

zebrafish_XP_068072896.1        QSQETENILYWINFIFIVAFTSEFVLKLFALRHYYFTNGWNIFDCVVVILSIVGMFLADL 1585
frog_XP_031751845.1             QSDYTDNVLYWINVVFIVFFTTECVLKLCALRHYYFTIGWNIFDFVVVILSIVGMFLADL 1612
human_sp|Q9UQD0.1|SCN8A_HUMAN   QSKQMENILYWINLVFVIFFTCECVLKMFALRHYYFTIGWNIFDFVVVILSIVGMFLADI 1605
mouse_sp|Q9WTU3.1|SCN8A_MOUSE   QSKQMENILYWINLVFVIFFTCECVLKMFALRHYYFTIGWNIFDFVVVILSIVGMFLADI 1603
                                **.  :*:*****.:*:: ** * ***: ******** ****** **************:

zebrafish_XP_068072896.1        IEKYFVSPTLFRVIRLARIGRILRLIKGAKGIRTLLFALMMSLPALFNIGLLLFLVMFIF 1645
frog_XP_031751845.1             ITKYFVSPTLFRVIRLARIGRILRLIKGAKGIRTLLFALMMSLPALFNIGLLLFLVMFIF 1672
human_sp|Q9UQD0.1|SCN8A_HUMAN   IEKYFVSPTLFRVIRLARIGRILRLIKGAKGIRTLLFALMMSLPALFNIGLLLFLVMFIF 1665
mouse_sp|Q9WTU3.1|SCN8A_MOUSE   IEKYFVSPTLFRVIRLARIGRILRLIKGAKGIRTLLFALMMSLPALFNIGLLLFLVMFIF 1663
                                * ************************************************************

zebrafish_XP_068072896.1        SIFGMSNFAYVKRESGIDDMYNFETFGNSMICLFMITTSAGWDGLLAPILNYPPDCEPTK 1705
frog_XP_031751845.1             SIFGMSNFAYVKKEAGIDDMFNFETFGNSMICLFQITTSAGWDGLLLPILNRPPDCDAHK 1732
human_sp|Q9UQD0.1|SCN8A_HUMAN   SIFGMSNFAYVKHEAGIDDMFNFETFGNSMICLFQITTSAGWDGLLLPILNRPPDCSLDK 1725
mouse_sp|Q9WTU3.1|SCN8A_MOUSE   SIFGMSNFAYVKHEAGIDDMFNFETFGNSMICLFQITTSAGWDGLLLPILNRPPDCSLDK 1723
                                ************:*:*****:************* ********** **** ****.  *

zebrafish_XP_068072896.1        ENPGTSVKGNCGNPSVGIFFFVMYIIVSFLIVVNMYIAIILENFSVATEESADPLCEDDF 1765
frog_XP_031751845.1             ENPGSQVKGDCGNPSVGIFFFVSYIIISFLIVVNMYIAIILENFSVATEESADPLSEDDF 1792
human_sp|Q9UQD0.1|SCN8A_HUMAN   EHPGSGFKGDCGNPSVGIFFFVSYIIISFLIVVNMYIAIILENFSVATEESADPLSEDDF 1785
mouse_sp|Q9WTU3.1|SCN8A_MOUSE   EHPGSGFKGDCGNPSVGIFFFVSYIIISFLIVVNMYIAIILENFSVATEESADPLSEDDF 1783
                                *:**: .**:************ ***:***************************.****

zebrafish_XP_068072896.1        ESFYEIWEKFDPTASQFITFAKLGDFADTLEHPLRVPKPNTIELIAMDLPMVSGDRIHCL 1825
frog_XP_031751845.1             ETFYEIWEKFDPDATQFIQFSKLPDFADALEHPLRIPKPNTIELIAMDLPMVSGDRIHCL 1852
human_sp|Q9UQD0.1|SCN8A_HUMAN   ETFYEIWEKFDPDATQFIEYCKLADFADALEHPLRVPKPNTIELIAMDLPMVSGDRIHCL 1845
mouse_sp|Q9WTU3.1|SCN8A_MOUSE   ETFYEIWEKFDPDATQFIEYCKLADFADALEHPLRVPKPNTIELIAMDLPMVSGDRIHCL 1843
                                *:********** *:*** :.** ****:******:************************
```

```
zebrafish_XP_068072896.1          DILFAFTKRVLGDSGDLDMMRQQMEERFIAANPSKVSFEPITTTLRRKQEHMSAGVIQRA 1885
frog_XP_031751845.1               DILFAFTKRVLGESGELDILRQQMEERFVASNPSKVSYEPITTTLRRKQEDVSAVVIQQA 1912
human_sp|Q9UQD0.1|SCN8A_HUMAN     DILFAFTKRVLGDSGELDILRQQMEERFVASNPSKVSYEPITTTLRRKQEEVSAVVLQRA 1905
mouse_sp|Q9WTU3.1|SCN8A_MOUSE     DILFAFTKRVLGDSGELDILRQQMEERFVASNPSKVSYEPITTTLRRKQEEVSAVVLQRA 1903
                                  ***********:**:**::********:*:******:***********.:** *:*:*

zebrafish_XP_068072896.1          FRAHLIRKGFICKRLLSSSRLENGGTNQDKKEGTPSTASLPSYDSVTKPEKEKLEESDS- 1944
frog_XP_031751845.1               YRRHLVKRGFISRKR-STGKMENGGTNMDKKEGTPSTASLPSYDSVTKPDKAKQERIEDA 1971
human_sp|Q9UQD0.1|SCN8A_HUMAN     YRGHLARRGFICKKT-TSNKLENGGTHREKKESTPSTASLPSYDSVTKPEKEKQQRAEEG 1964
mouse_sp|Q9WTU3.1|SCN8A_MOUSE     YRGHLARRGFICRKI-TSNKLENGGTHREKKESTPSTASLPSYDSVTKPDKEKQQRAEEG 1962
                                  :* ** ::***.::  ::.::*****: :***.****************:* * :. :.

zebrafish_XP_068072896.1          KGKKGKNQKDVKESKF     1960
frog_XP_031751845.1               IRERAKKQKSVRESKC     1987
human_sp|Q9UQD0.1|SCN8A_HUMAN     RRERAKRQKEVRESKC     1980
mouse_sp|Q9WTU3.1|SCN8A_MOUSE     RRERAKRQKEVRESKC     1978
                                    ::.*.**.*:***
```

Figure 3. Multiple protein alignment of Nav1.6. Each row represents the Nav1.6 protein from a different species, while each column corresponds to a specific amino acid position in the aligned sequences. Conservation levels are indicated by symbols below each column: "*" denotes positions where all species have identical amino acids (complete conservation), ":" indicates positions with strongly similar amino acid properties (such as basic or acidic residues), "." marks positions with weakly similar properties, and spaces represent positions with no significant similarity across species. Background coloring reflects amino acid chemical properties: red indicates basic residues (K, R, H), blue indicates acidic residues (D, E), green indicates polar residues (S, T, N, Q), yellow/orange indicates hydrophobic residues (A, V, L, I, M, F, W), and purple indicates residues with special structural properties (G, P, C). This dual annotation system allows identification of both evolutionary conservation patterns and the biochemical nature of sequence variations.

these domains govern voltage sensing and sodium ion selectivity. Conserved elements such as the DEKA selectivity filter—a ring of four amino acid residues (aspartic acid, glutamic acid, lysine, and alanine) that creates a negatively charged binding site for sodium ion selectivity—are clearly preserved across species (15). These highly conserved core functional elements (>95% amino acid identity) should be avoided as therapeutic targets due to the high probability of disrupting essential channel function.

In contrast, cytoplasmic domains show greater variability. Specifically, the N-terminal region containing the MAP1B binding site (residues 77-80, VAVP motif) displays moderate conservation, while the C-terminal region containing the FGF14 interaction domain shows similar variability. These regulatory regions, which mediate protein-protein interactions that control channel trafficking and localization, display conservation patterns indicating they can tolerate selective disruption without eliminating basic channel function. This observation supports trafficking-based targeting given the proven success of similar approaches for Nav1.7 (8-10) and the functional parallels between CRMP2-Nav1.7 and MAP1B-Nav1.6 regulatory mechanisms.

Protein-Protein Interaction (PPI) map of Nav1.6 (SCN8A)

To identify molecules that might modulate Nav1.6 (SCN8A) localization, gating, and surface availability in DRGs, influencing excitability and the threshold for extracellular stimulation, a protein--protein interaction (PPI) network was utilized on Nav1.6 (Figure 4). The network integrates curated experimental data and high-confidence predicted associations, and was visualized to highlight functional clusters (channel subunits and modulators, cytoskeletal anchors, trafficking/adaptor proteins, and regulatory enzymes). Examining these links to molecular mechanisms (anchoring at the axon initial segment, trafficking to the membrane, and post-translational regulation) that can change spike threshold

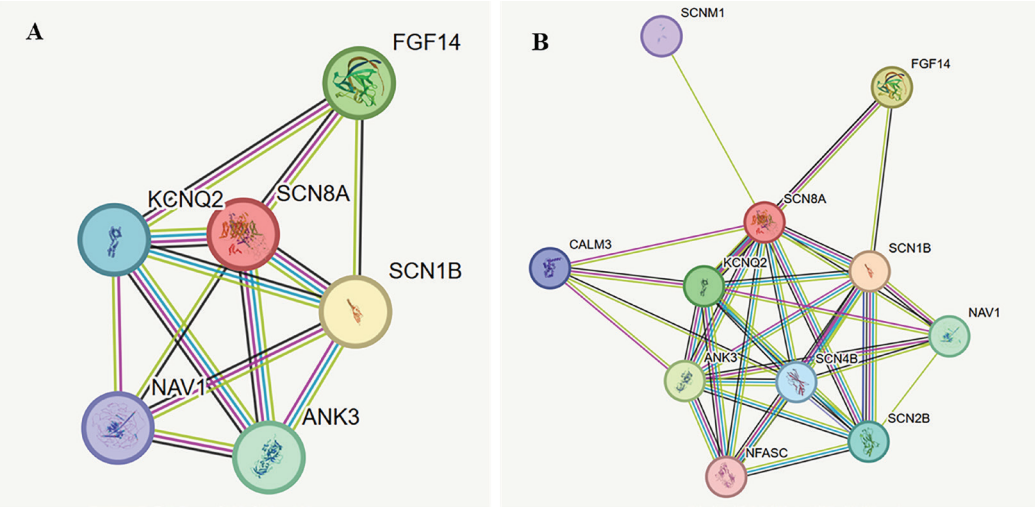

Figure 4. Nav1.6 Protein-Protein Interaction Networks (Simplified and Comprehensive Views). (A) presents a simplified network illustrating the most significant direct interactions with Nav1.6. **(B)** provides a comprehensive network view, including additional partners and secondary interactions, revealing the broader regulatory and structural context of Nav1.6 function. In both networks, Nav1.6 is shown as the central node, with surrounding nodes representing proteins that are functionally or physically associated with it. Edge thickness corresponds to interaction confidence (thicker edges indicate higher combined scores), and edge colors denote the primary evidence channel following STRING conventions: green = neighborhood, red = gene fusion, blue = co-occurrence, purple = experimental, yellow = text-mining, light-blue = database, and black = coexpression.

and firing patterns provides insight into how Nav1.6 regulation influences neuronal excitability; identifying such partners helps prioritize molecular targets for trafficking-based therapeutic interventions.

The network shows a tight cluster of ankyrin-G (ANK3) and β-spectrin-family proteins closely linked to Nav1.6, consistent with established roles in anchoring sodium channels at the axon initial segment and nodes of Ranvier; disruption of these scaffolds displaces Nav1.6 and alters excitability (16, 17). Auxiliary β subunits and FGF family members (e.g. FGF14/FGF12) cluster near the alpha subunit, indicating partners known to modulate channel gating and surface expression. These proteins are candidate modulators whose expression or function could shift activation thresholds. Microtubule-associated proteins such as MAP1B (detected in experimental interaction screens) connect to Nav1.6 and suggest interactions with the trafficking machinery; these partners could influence delivery or retention of channels at the membrane (11).

Of particular therapeutic relevance, MAP1B's interaction with Nav1.6 extends beyond structural anchoring to active regulation of channel surface availability. O'Brien *et al* (11) identified MAP1B binding to the VAVP motif (residues 77-80) in the Nav1.6 N-terminus, and subsequent work by Solé *et al* (12) demonstrated that this interaction prevents compartment-specific endocytosis of Nav1.6 at the axon initial segment. Disruption of the MAP1B-Nav1.6 interaction (via VAVP77-80AAAA mutation) increases endocytosis and substantially reduces Nav1.6 surface expression at the axon initial segment (11, 12). Given the success of CRMP2-Nav1.7 trafficking disruption (8-10) as a therapeutic strategy, we investigated whether Nav1.6 possesses similar regulatory properties amenable to trafficking-based modulation. The prominence of MAP1B in the Nav1.6 interaction network, combined with experimental evidence that MAP1B disruption achieves ~40% surface expression reduction (12), a magnitude that falls within the therapeutic range identified by the computational modeling, demonstrates that trafficking modulation represents a viable alternative to direct channel blockade.

The PPI map highlights a core module of scaffolding and trafficking proteins (ANK3, β-spectrin family, MAP1B) that likely determine Nav1.6 localization at the AIS and thereby strongly influence spike initiation threshold; a second module of auxiliary subunits and FGFs is positioned to adjust channel gating. Together these modules provide mechanistic targets for trafficking-based interventions intended to modulate DRG excitability (11, 16).

Expression profile of SCN8A

The expression data of SCN8A was retrieved from the MARRVEL>GTEX database (Figure 5). The graph shows the transcript abundance as transcripts per million (TPM) across a broad panel of tissues: this reveals the tissue specificity and relative magnitude of SCN8A expression, helping to place expression in the context of other CNS and peripheral tissues. Knowing where SCN8A is highly expressed (and where it is low or absent) informs whether DRGs are likely to depend on Nav1.6 for action-potential initiation and helps prioritize tissues and cell types for targeted follow-up using single-cell approaches or functional assays.

SCN8A displays marked enrichment in central nervous system tissues (multiple brain subregions), consistent with Nav1.6's known neuronal role. Peripheral tissues show low or near-zero TPM in most cases. From these bulk tissue data alone, SCN8A is confirmed as a CNS-enriched gene. However, bulk tissue measurements cannot resolve cell-type-specific expression patterns. Importantly, dorsal root ganglia—the primary sensory neurons implicated in neuropathic pain—are not adequately represented in the GTEx dataset, limiting conclusions about Nav1.6 expression in the specific cell populations most relevant to pain signaling. Single-cell RNA sequencing studies of DRG neurons would be required to characterize Nav1.6 expression in pain-relevant neuronal subtypes with appropriate resolution (18).

Computer model of pain-sensing neuron with varying expressions of Nav1.6

To investigate how Nav1.6 expression levels affect neuronal excitability in neuropathic pain conditions, simple computational models were developed of dorsal root ganglion (DRG) neurons with varying Nav1.6 expression levels (19). Based on established Hodgkin-Huxley formulations and experimental parameters from the literature, four conditions were simulated: normal expression (1.0x), increased expression typical of neuropathic conditions (1.5x), decreased expression (0.7x), and near-knockout levels (0.1x) (Figure 6).

The 0.7x condition represents a ~30% reduction that eliminates pathological repetitive firing while preserving normal responsiveness. Experimental disruption of MAP1B-Nav1.6 interaction produces ~40% reduction in surface expression at the axon initial segment (12), indicating that the magnitude of reduction achieved through MAP1B-Nav1.6 disruption falls within the range the modeling identifies as reducing hyperexcitability while preserving normal responsiveness.

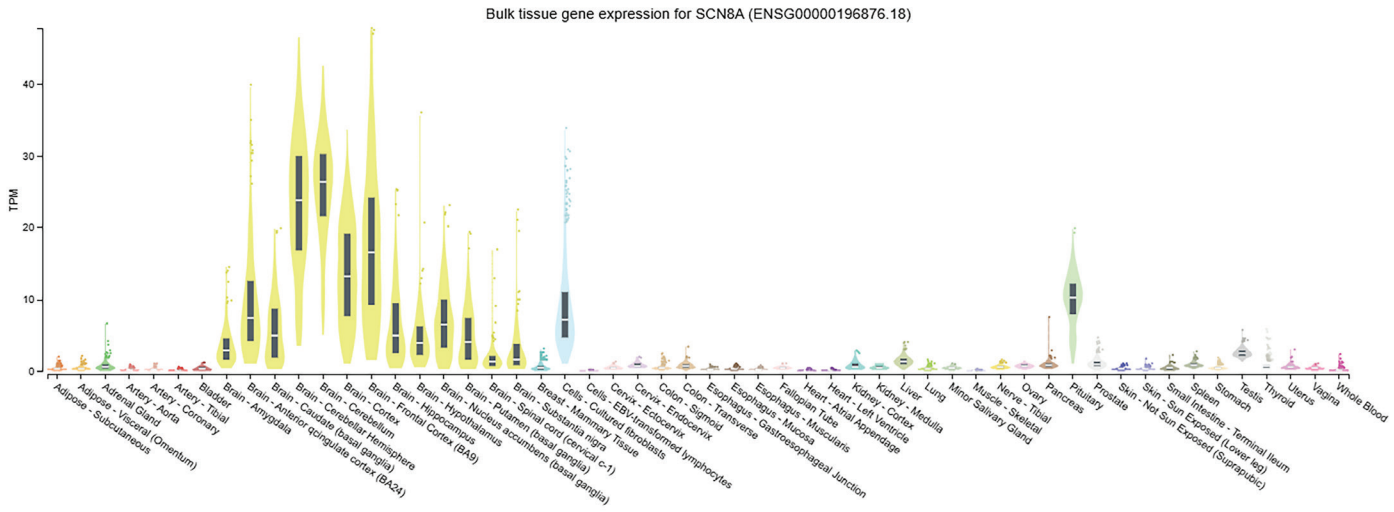

Figure 5. Tissue-specific expression profile of SCN8A across human tissues. Violin plots showing SCN8A transcript abundance measured as transcripts per million (TPM) across 54 human tissue types from the GTEx database. Each violin represents the distribution of sample-level expression values for that tissue, with the central box and line indicating the interquartile range and median, respectively. The x-axis displays tissue types with labels plotted diagonally for clarity. The y-axis shows transcript abundance in TPM, with values ranging from 0 to 40. Note the marked enrichment in central nervous system tissues (brain subregions) compared to peripheral tissues.

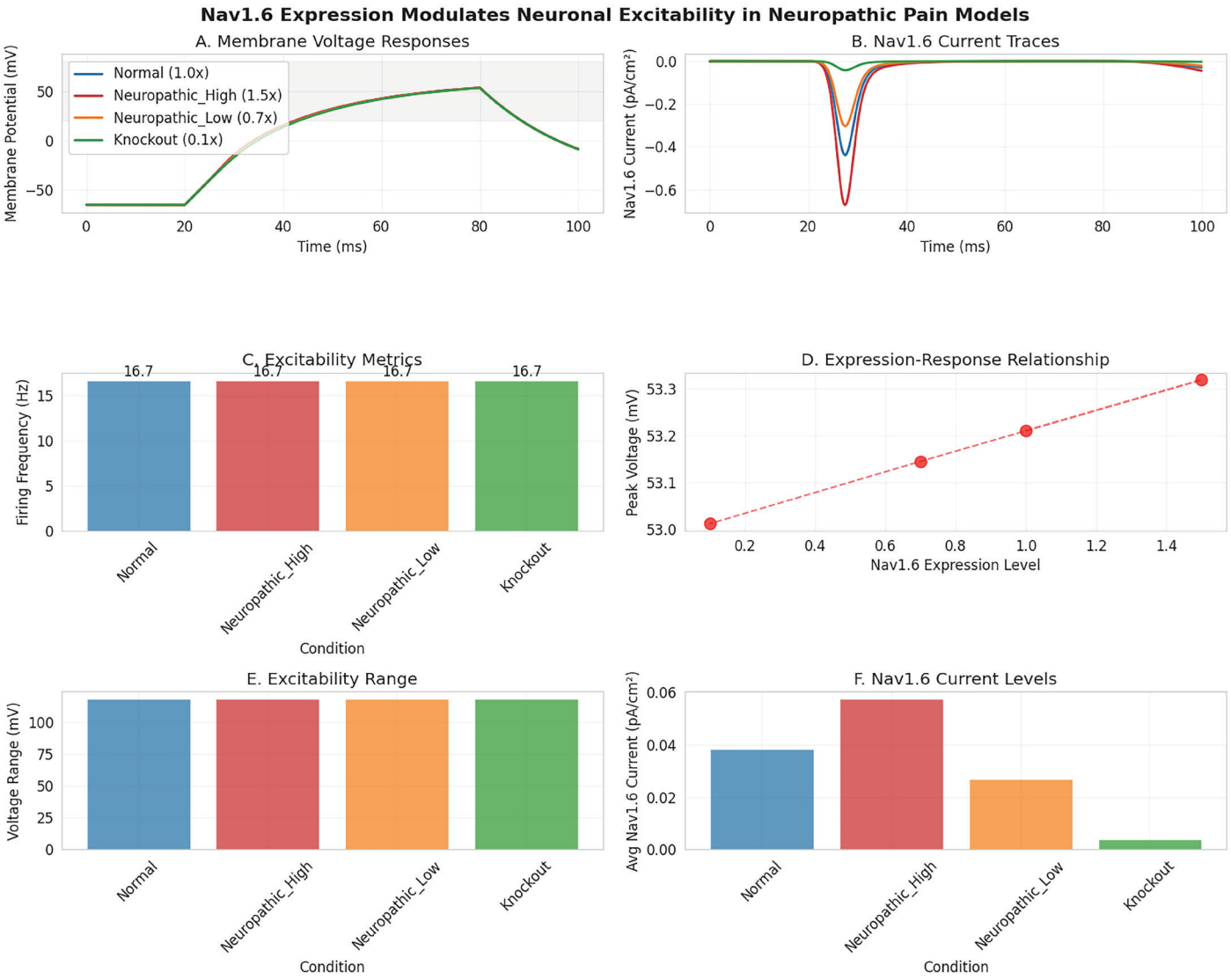

Figure 6. Nav1.6 expression levels critically determine neuronal excitability patterns. Panel A shows membrane voltage responses to standardized current injection, revealing that increased Nav1.6 expression (red trace) produces multiple action potentials compared to single spikes in normal conditions (blue trace). Panel B illustrates corresponding Nav1.6 current traces, showing enhanced and prolonged inward currents in neuropathic conditions. Panel C quantifies firing frequency differences, demonstrating a clear relationship between Nav1.6 expression and neuronal hyperexcitability. Panel D establishes the expression-response relationship, showing peak voltage responses scale with Nav1.6 levels. Panel E compares spike amplitudes across conditions, while Panel F illustrates the Nav1.6 Current Levels for Nav1.6-targeted interventions. These results support the hypothesis that modulating Nav1.6 expression may provide therapeutic benefits for neuropathic pain management.

DISCUSSION

Context and Therapeutic Landscape

This computational study systematically evaluated Nav1.6 (SCN8A) as a candidate for trafficking-based therapeutic modulation in neuropathic pain. By integrating structural prediction, evolutionary conservation, protein interaction networks, expression profiling, and electrophysiological modeling, we established that Nav1.6 possesses molecular properties enabling trafficking-based therapeutic modulation, using the established Nav1.7-CRMP2 system as conceptual guide for an alternative to direct channel blockade.

Current neuropathic pain treatments remain

inadequate, with first-line therapies including gabapentinoids achieving meaningful pain relief (≥50% reduction) in only approximately 30-35% of patients (6, 7). Voltage-gated sodium channels have been intensively pursued as therapeutic targets, with Nav1.7 attracting extensive pharmaceutical investment based on compelling genetic validation from human pain disorders. However, clinical translation has proven challenging: Pfizer's PF-05089771 failed to meet efficacy endpoints in diabetic peripheral neuropathy Phase II trials, and Convergence/Biogen's CNV1014802 showed limited efficacy in trigeminal neuralgia (20). Trafficking disruption represents an established therapeutic strategy for Nav1.7, where peptides and small molecules that disrupt the CRMP2-Nav1.7 interaction reduce channel surface expression through endocytosis modulation and alleviate pain in preclinical models (8-10). These disappointing outcomes have prompted exploration of alternative sodium channel targets and therapeutic modalities.

Nav1.6 has emerged as an alternative candidate based on its substantial contribution (up to 60%) to tetrodotoxin-sensitive sodium current in large DRG neurons, preferential accumulation at injury sites, and involvement in both mechanical and chemotherapy-induced neuropathic pain (3, 4). A selective Nav1.6 inhibitor (NBI-921352) is currently in Phase II clinical trials for epilepsy (5), demonstrating the feasibility of subtype-selective targeting. However, alternative therapeutic approaches beyond direct channel blockade have not been systematically explored for Nav1.6.

Trafficking Disruption as an Unexplored Strategy for Nav1.6

Trafficking disruption represents an established therapeutic strategy for Nav1.7, where peptides and small molecules that disrupt the CRMP2-Nav1.7 interaction reduce channel surface expression through endocytosis modulation and alleviate pain in preclinical models (8-10). This approach offers theoretical advantages over direct channel blockade: partial reduction of surface expression rather than complete functional inhibition, targeting of a regulatory mechanism rather than the channel pore, and potential for superior isoform selectivity.

Nav1.6 engages in regulatory interactions that control surface expression through MAP1B binding, which prevents endocytosis and maintains channel availability (11, 12). Experimental disruption substantially reduces surface expression at the axon initial segment (12). Like CRMP2's regulation of Nav1.7, MAP1B prevents Nav1.6 endocytosis and maintains surface channel availability.

Despite this characterized regulatory mechanism, trafficking disruption has not been proposed as a therapeutic approach for Nav1.6-mediated neuropathic pain. The computational analysis provides converging evidence validating this strategy. Both Nav1.6 and Nav1.7 contribute to DRG hyperexcitability in neuropathic conditions, establishing a similar therapeutic rationale. The Hodgkin-Huxley modeling demonstrates that ~30% Nav1.6 reduction (0.7x expression condition) eliminates repetitive firing characteristic of neuropathic states while preserving single action potential responses to physiological stimuli (Figure 6). Experimental MAP1B-Nav1.6 disruption produces ~40% reduction in surface expression at the axon initial segment, a magnitude comparable to the reduction level the modeling identifies as eliminating hyperexcitability while preserving responsiveness (12). This correspondence between experimentally achievable and computationally effective reduction levels validates trafficking disruption as a therapeutic approach. Nav1.6's CNS-enriched expression pattern (Figure 5) offers potential selectivity advantages, though GTEx bulk tissue data inadequately represent dorsal root ganglia (discussed in Limitations).

Considerations for Nav1.6 Trafficking Disruption

Nav1.6-MAP1B trafficking regulation has been characterized (11, 12), but its therapeutic potential remains unexplored. The success of CRMP2-Nav1.7 trafficking disruption provides precedent for this approach, though several mechanistic considerations inform therapeutic development:

Several mechanistic parallels to the Nav1.7 precedent support this approach. MAP1B regulates Nav1.6 surface expression through endocytosis modulation (12). The CRMP2-Nav1.7 system operates through a similar mechanism where trafficking protein binding prevents endocytosis. Both binding sites are located in accessible cytoplasmic domains (N-terminus for MAP1B-Nav1.6, C-terminus for CRMP2-Nav1.7). Both interactions maintain channel availability at functionally relevant subcellular locations (axon initial segment for Nav1.6, peripheral axons for Nav1.7). Both channels contribute to DRG hyperexcitability in neuropathic pain states.

However, key distinctions warrant consideration. MAP1B has broader expression and multiple cellular functions beyond Nav1.6 regulation, including microtubule stabilization and axonal transport, potentially creating off-target liability not present for CRMP2-Nav1.7 targeting. In contrast, CRMP2's role

is more specific to channel regulation. The binding interfaces differ structurally: MAP1B recognizes a short linear motif (VAVP), while CRMP2 interactions involve more extensive protein-protein interfaces. This difference influences the molecular design requirements for selective disruptor molecules but does not preclude therapeutic development. Additionally, MAP1B-Nav1.6 disruption has been characterized primarily at the axon initial segment in central neurons, whereas pain-relevant effects would occur in DRG peripheral terminals, requiring validation that trafficking mechanisms are conserved across these subcellular compartments.

The GTEx expression profile (Figure 5) shows Nav1.6 enrichment in CNS tissues with low expression in skeletal muscle and heart. However, as detailed in Results and Limitations, GTEx inadequately represents dorsal root ganglia. While low expression in muscle (Nav1.4-enriched) and heart (Nav1.5-enriched) suggests potential to avoid some side effects, DRGs are anatomically peripheral, creating uncertainty about true selectivity. Without DRG-specific expression data, selectivity claims remain speculative. Ongoing clinical development of direct Nav1.6 inhibitors (NBI-921352) validates Nav1.6 as a therapeutic target; trafficking-based approaches represent a complementary strategy with distinct pharmacological profiles, offering partial reduction of channel availability rather than complete blockade.

Limitations and Appropriate Interpretation

This computational study evaluates trafficking-based Nav1.6 modulation based on quantitative modeling and characterized regulatory mechanisms. Several limitations of the computational approach warrant explicit acknowledgment and guide future experimental validation.

Computational modeling assumptions: The Hodgkin-Huxley simulations employed simplifying assumptions, including uniform Nav1.6 distribution across the neuronal membrane, whereas experimental evidence demonstrates channel clustering at specific subcellular locations (axon initial segment, nodes of Ranvier). The model focused exclusively on Nav1.6 channels, while DRG neurons express multiple sodium channel subtypes (Nav1.1, Nav1.6, Nav1.7, Nav1.8, Nav1.9) that contribute differentially to excitability. The simulation used static parameters, whereas neuropathic pain involves dynamic changes in channel expression, localization, and biophysical properties over time. Despite these limitations, the model provides valuable insights into the basic relationship between Nav1.6 expression levels and excitability patterns.

Expression data resolution: GTEx bulk tissue measurements confirm CNS enrichment but cannot resolve cell-type-specific expression in pain-relevant DRG neuron subtypes. The dataset inadequately represents dorsal root ganglia, limiting conclusions about Nav1.6's role in specific nociceptive versus non-nociceptive sensory neurons. Single-cell RNA sequencing of human DRG tissue would be required to address this limitation.

Trafficking mechanism validation: While MAP1B-Nav1.6 interaction has been characterized at the axon initial segment in central neurons, direct experimental evidence for similar trafficking regulation in DRG peripheral terminals is lacking. The therapeutic hypothesis assumes conservation of this mechanism across subcellular compartments, requiring validation in pain-relevant contexts.

Off-target considerations: MAP1B has multiple cellular functions beyond Nav1.6 regulation. Therapeutic approaches targeting this interaction would require careful assessment of selectivity and potential effects on other MAP1B-dependent processes. The feasibility of developing molecules that selectively disrupt MAP1B-Nav1.6 interaction without affecting other MAP1B functions remains to be determined.

Clinical translation uncertainty: This computational framework generates testable hypotheses but does not experimentally validate therapeutic efficacy. The relationship between partial Nav1.6 reduction and pain relief in animal models requires direct experimental testing.

Future Experimental Directions

The computational analyses establish specific experimental priorities for validating and advancing trafficking disruption as a therapeutic approach. Preclinical validation in neuropathic pain models will test whether MAP1B-Nav1.6 disruption reduces pain behaviors, building on the modeling demonstration that ~30% Nav1.6 reduction eliminates repetitive firing in DRG neurons while experimental MAP1B disruption achieves ~40% surface expression reduction (12)—a magnitude within the range the computational analysis identifies as reducing hyperexcitability. Specificity assessment must determine whether MAP1B-targeted approaches have acceptable off-target effects given MAP1B's multiple cellular functions, which could be addressed through conditional knockout studies or highly selective disruptor molecules. Mechanistic studies should

validate whether trafficking disruption in DRG neurons produces effects comparable to those characterized at the axon initial segment, with single-cell electrophysiology combined with surface biotinylation quantifying changes in channel availability. Therapeutic development requires identifying peptides, peptidomimetics, or small molecules that selectively disrupt MAP1B-Nav1.6 interaction, where structure-based drug design approaches could leverage the characterized VAVP binding motif. Finally, comparative studies with direct channel inhibitors (NBI-921352) would determine whether trafficking-based approaches offer distinct therapeutic advantages in terms of efficacy, side effect profiles, or patient populations.

CONCLUSION

This computational integration evaluates Nav1.6 trafficking disruption as a candidate therapeutic strategy for neuropathic pain through systematic analysis of structural features, evolutionary conservation, protein interaction networks, expression profiling, and electrophysiological modeling. Through transmembrane prediction, conservation analysis, protein interaction mapping, expression profiling, and electrophysiological modeling, we identified several key findings:

First, MAP1B-Nav1.6 interaction represents a characterized regulatory node controlling channel surface expression through endocytosis modulation (12), providing a defined molecular target with functional parallels to the CRMP2-Nav1.7 system. Second, the MAP1B binding site displays moderate conservation contrasting with highly conserved pore domains, indicating potential tolerance for selective disruption. Third, computational modeling demonstrates that ~30% Nav1.6 reduction (0.7x expression) eliminates repetitive firing while preserving single action potential generation in simulated DRG neurons. Experimental MAP1B-Nav1.6 disruption achieves ~40% surface expression reduction, a magnitude comparable to the reduction level the modeling identifies as eliminating hyperexcitability while preserving responsiveness (12). Fourth, CNS-enriched expression patterns suggest potential selectivity advantages, though DRG-specific expression requires validation with higher-resolution methods.

This computational study predicts therapeutic efficacy for MAP1B-Nav1.6. However, experimental validation in animal pain models remains essential to confirm these predictions. As direct channel blockers for Nav1.7 have faced clinical challenges despite strong genetic validation, alternative approaches targeting channel regulation rather than channel function may offer improved therapeutic profiles for neuropathic pain management.

This work establishes trafficking disruption as a computationally validated strategy for Nav1.6 modulation, with three specific testable predictions: (1) MAP1B-Nav1.6 disruption will reduce DRG excitability without eliminating responsiveness, as the modeling demonstrates that ~30% Nav1.6 reduction eliminates repetitive firing while preserving single action potentials; (2) peptides targeting the VAVP binding motif (residues 77-80) will achieve the ~40% surface expression reduction demonstrated experimentally with genetic disruption (12); and (3) this magnitude of reduction will alleviate neuropathic pain behaviors in preclinical models. The quantitative alignment between existing experimental tools and the computational predictions provides a direct path from in silico modeling to experimental validation, positioning trafficking-based approaches as a complementary strategy to traditional channel blockers for neuropathic pain.

ACKNOWLEDGEMENT

I would like to express my sincere gratitude to my research mentor, Dr. Ozturk, for their guidance throughout this study. Her endless patience with me has left me extremely grateful. I am especially thankful for her assistance in navigating the complexities of bioinformatics analysis and her constructive feedback that helped build and refine my paper. This research would not have been possible without her mentorship and encouragement.

FUNDING SOURCES

No funding was received for the conduct of this research or preparation of this article.

CONFLICT OF INTEREST

The author declares no conflicts of interest related to this work.

REFERENCES

1. van Hecke O, *et al*. Neuropathic pain in the general population: a systematic review of epidemiological studies. *Pain*. 2014; 155 (4): 654-62. https://doi.org/10.1016/j.pain.2013.11.013

2. Boiko T, *et al*. Functional specialization of the axon initial segment by isoform-specific sodium channel targeting. *J Neurosci*. 2003; 23 (6): 2306-13. https://doi.org/10.1523/JNEUROSCI.23-06-02306.2003
3. Chen L, *et al*. Conditional knockout of NaV1.6 in adult mice ameliorates neuropathic pain. *Sci Rep*. 2018; 8 (1): 3845. https://doi.org/10.1038/s41598-018-22216-w
4. Sittl R, *et al*. Anticancer drug oxaliplatin induces acute cooling-aggravated neuropathy via sodium channel subtype NaV1.6-resurgent and persistent current. *Proc Natl Acad Sci U S A*. 2012; 109 (17): 6704-9. https://doi.org/10.1073/pnas.1118058109
5. Johnson JP, *et al*. NBI-921352, a first-in-class, NaV1.6 selective, sodium channel inhibitor that prevents seizures in Scn8a gain-of-function mice, and wild-type mice and rats. *eLife*. 2022; 11: e72468.
6. Wiffen PJ, *et al*. Gabapentin for chronic neuropathic pain in adults. *Cochrane Database Syst Rev*. 2017; 6 (6): CD007938. https://doi.org/10.1002/14651858.CD003726.pub4
7. Finnerup NB, *et al*. Pharmacotherapy for neuropathic pain in adults: a systematic review and meta-analysis. *Lancet Neurol*. 2015; 14 (2): 162-73. https://doi.org/10.1016/S1474-4422(14)70251-0
8. Dustrude ET, *et al*. CRMP2 protein SUMOylation modulates NaV1.7 channel trafficking. *J Biol Chem*. 2013; 288 (34): 24316-31. https://doi.org/10.1074/jbc.M113.474924
9. Dustrude ET, *et al*. Hierarchical CRMP2 posttranslational modifications control NaV1.7 function. *Proc Natl Acad Sci U S A*. 2016; 113 (52): E8443-E8452. https://doi.org/10.1073/pnas.1610531113
10. Gomez K, *et al*. Identification and targeting of a unique NaV1.7 domain driving chronic pain. *Proc Natl Acad Sci U S A*. 2023; 120 (31): e2217800120. https://doi.org/10.1073/pnas.2217800120
11. O'Brien JE, *et al*. Interaction of voltage-gated sodium channel Nav1.6 (SCN8A) with microtubule-associated protein Map1b. *J Biol Chem*. 2012; 287 (22): 18459-66. https://doi.org/10.1074/jbc.M111.336024
12. Solé L, *et al*. The MAP1B binding domain of Nav1.6 is required for stable expression at the axon initial segment. *J Neurosci*. 2019; 39 (22): 4238-51. https://doi.org/10.1523/JNEUROSCI.2771-18.2019
13. Hodgkin AL, Huxley AF. A quantitative description of membrane current and its application to conduction and excitation in nerve. *J Physiol*. 1952; 117 (4): 500-44. https://doi.org/10.1113/jphysiol.1952.sp004764
14. Rush AM, *et al*. Electrophysiological properties of two axonal sodium channels, Nav1.2 and Nav1.6, expressed in mouse spinal sensory neurons. *J Physiol*. 2005; 564 (3): 803-15. https://doi.org/10.1113/jphysiol.2005.083089
15. Sun YM, *et al*. On the structural basis for size-selective permeation of organic cations through the voltage-gated sodium channel. Effect of alanine mutations at the DEKA locus on selectivity, inhibition by Ca^{2+} and H^{+}, and molecular sieving. *J Gen Physiol*. 1997; 110 (6): 693-715. https://doi.org/10.1085/jgp.110.6.693
16. Zybura A, *et al*. Distinctive properties and powerful neuromodulation of Nav1.6 sodium channels regulates neuronal excitability. *Cells*. 2021; 10 (7): 1595. https://doi.org/10.3390/cells10071595
17. Jenkins SM, Bennett V. Ankyrin-G coordinates assembly of the spectrin-based membrane skeleton, voltage-gated sodium channels, and L1 CAMs at Purkinje neuron initial segments. *J Cell Biol*. 2001; 155 (5): 739-46. https://doi.org/10.1083/jcb.200109026
18. The Human Protein Atlas. Tissue expression of SCN8A - Summary (Internet). Available from: https://www.proteinatlas.org/ENSG00000196876-SCN8A/tissue (accessed on 2025-08-28)
19. Kan P, *et al*. Computational modeling to study the impact of changes in Nav1.8 sodium channel on neuropathic pain. *Front Comput Neurosci*. 2024; 18: 1327986. https://doi.org/10.3389/fncom.2024.1327986
20. McDonnell A, *et al*. Efficacy of the Nav1.7 blocker PF-05089771 in a randomized, placebo-controlled, double-blind clinical study in subjects with painful diabetic peripheral neuropathy. *Pain*. 2018; 159 (8): 1465-76. https://doi.org/10.1097/j.pain.0000000000001227

SUPPLEMENTARY MATERIAL

https://github.com/Commmet/Investigation-into-Nav1.6.-And-its-potential-therapeutic-benefits-supplementary-code.git

Supplementary 1. The code that was used to generate Figure 6. Python (version 3.8) was used to create the Hodgkin-Huxley simulated model with parameters based on literature that used similar computational simulations (19). The implementation utilized NumPy (version 1.21.0) for numerical computations, Matplotlib (version 3.4.3) and Seaborn (version 0.11.2) for visualization, and SciPy (version 1.7.0) for numerical integration. The model makes several simplifying assumptions: uniform Nav1.6 distribution across the membrane (actual channels cluster at specific nodes), simplified neuronal morphology without dendritic arbors, constant temperatures and ionic concentrations throughout simulation, and absence of other sodium channel subtypes (Nav1.1, Nav1.7, Nav1.8, Nav1.9) that contribute to DRG excitability. AI assistance was used for code development, debugging, and optimization. All simulations were executed using Google Colab cloud computing environment.